Journal of Rock Mechanics and Geotechnical Engineering 15 (2023) 2250–2263

Contents lists available at ScienceDirect

Journal of Rock Mechanics and Geotechnical Engineering

journal homepage: www.jrmge.cn

Full Length Article

Influence of uncertainties: A focus on block volume and shape assessment for rockfall analysis

Gessica Umili*, Battista Taboni, Anna Maria Ferrero

Department of Earth Sciences, University of Turin, via Valperga Caluso 35, 10125, Turin, Italy

ARTICLE INFO

Article history:
Received 30 November 2022
Received in revised form
27 February 2023
Accepted 12 March 2023
Available online 12 May 2023

Keywords:
Rockfall
In situ block size distribution (IBSD)
Block
Volume
Shape
Uncertainty

ABSTRACT

Block size and shape depend on the state of fracturing of the rock mass and, consequently, on the geometrical features of the discontinuity sets (mainly orientation, spacing, and persistence). The development of non-contact surveying techniques applied to rock mass characterization offers significant advantages in terms of data numerosity, precision, and accuracy, allowing for performing a rigorous statistical analysis of the database. This fact is particularly evident when dealing with rockfall phenomena: uncertainties in spacing and orientation data could significantly amplify the uncertainties connected with in situ block size distribution (IBSD), which represents a relation between each possible value of the volume and its probability of not being exceeded. In addition to volume, block shape can be considered as a derived parameter that suffers from uncertainties. Many attempts to model the possible trajectories of blocks considering their actual shape have been proposed, aiming to reproduce the effect on motion. The authors proposed analytical equations for calculating the expected value and variance of volume distributions, based on the geometrically correct equation for block volume in the case of three discontinuity sets. They quantify and discuss the effect of both volume and shape variability through a synthetic case study. Firstly, a fictitious rock mass with three discontinuity sets is assumed as the source of rockfall. The IBSDs obtained considering different spacing datasets are quantitatively compared, and the overall uncertainty effect is assessed, proving the correctness of the proposed equations. Then, block shape distributions are obtained and compared, confirming the variability of shapes within the same IBSD. Finally, a comparison between trajectory simulations on the synthetic slope is reported, aiming to highlight the effects of the propagation of uncertainties to block volume and shape estimation. The benefits of an approach that can quantify the uncertainties are discussed from the perspective of improving the reliability of simulations.

1. Introduction

The recent evolution of non-contact surveying techniques for rock mass characterization offers significant advantages in many aspects. In particular, in terms of numerosity, precision, and accuracy of the geometrical data of discontinuities (orientation, spacing, trace length), the non-contact survey has proved to be highly effective (Riquelme et al., 2017; Kong et al., 2020). However, the potential benefits of such databases can be lost without rigorous statistical analysis (Carriero et al., 2021). The variability of the properties of natural complex materials, such as rock masses, defines an initial level of uncertainty that cannot be removed as an inherent material feature. This uncertainty is usually referred to as aleatoric (Baecher and Christian, 2003). On the other hand, the variability of the measures of a given property is influenced by the level of knowledge; this uncertainty is known as epistemic, and it can be reduced by increasing the quantity and quality of data describing the considered property (Ferrero et al., 2016). This process, however, cannot be performed without employing a rigorous statistical approach and treatment of the data. Otherwise, even more uncertainties could be introduced. In fact, poor treatment of data could significantly amplify the uncertainties associated with the assessment of representative results (e.g. mean orientation of principal discontinuity sets, mean corrected spacing), and ultimately affect derived data (e.g. block volume and shape) and results of modeling.

* Corresponding author.
E-mail address: gessica.umili@unito.it (G. Umili).
Peer review under responsibility of Institute of Rock and Soil Mechanics, Chinese Academy of Sciences.

https://doi.org/10.1016/j.jrmge.2023.03.016

In rockfall analysis, epistemic uncertainty affects the rockfall source's location and volume, the topographic data's scale or resolution, the modeling method's selection, and the parameters used for modeling. Aleatory uncertainty affects the topography of the slope and the mechanical properties of the rockfall source areas, which are dependent on factors such as lithology, random distribution of fractures in the rock, and geological movement experience (Wang et al., 2014). Statistical tests are strongly encouraged to evaluate the best-fitting distributions to reduce epistemic errors in surveyed data (Umili et al., 2020). As the cumulative distribution function (CDF) of block volume associates each value with a probability of not being exceeded (Stavropoulou, 2014), building a reliable and comprehensive distribution is fundamental.

Since volume depends on orientation and spacing variability, the sampled data of each discontinuity set should contain a statistically sufficient number of measurements and represent the variability in the considered rock mass. Therefore, the larger the maximum spacing, the greater the area that needs to be considered to collect sufficient measurements (Ferrero et al., 2016; Umili et al., 2020). In addition to volume, block shape could also be considered a derived parameter that suffers from uncertainties. Although the lumped mass method is still the most commonly employed in rockfall analysis, many attempts to model block trajectories taking into account their actual shape have been proposed. These methods aim to reproduce the effect of block shape on motion and provide more accurate simulations. The level of details can vary, from methods that can properly model rigid bodies only if dealing with simplified geometries, where the block shape is reduced to a sphere, a disc, an ellipsoid, or a prism (Dorren, 2016), to other more advanced and complex methods where it is possible to employ even digital models of the actual block to define its geometry (Leine et al., 2014, 2021; Noël et al., 2016, 2021). These aspects are worth investigating when dealing with block volume and shape selection aiming at the design of protection works. If, on the one hand, the engineering approach to rockfall problems needs to facilitate the identification of design parameters, on the other hand, a high level of simplification could mask the ripple effect of uncertainties on the reliability of the results (Carriero et al., 2023). Caviezel et al. (2021) defined rockfall hazard scenarios via both block sizes and shapes, incorporating a set of site-specific, realistic rock shapes in hazard assessments.

In this paper, the analytical equations are proposed for calculating the expected value and the variance of volume distributions based on the geometrically correct equation for calculating block volume in the case of three intersecting discontinuity sets. Then, we quantify and discuss the effect of both volume and shape variability through a synthetic case study. Essentially, it consists of a rock face and the underlying slope, fully known in terms of geometrical features. By assuming different spacing datasets with variable average values and variances, the block volume CDFs and the shape distributions are determined, and the overall uncertainty effect is assessed. Then, rockfall trajectory simulations are reported, aiming to highlight the possible effect of the involved uncertainties and the potential benefits of a rigorous approach for improving the reliability of rockfall analysis.

2. Material and methods

2.1. Block volume

The number, spacing, and persistence of discontinuity sets determine block dimensions. The number of sets and their orientation establish the shape of the resulting blocks (ISRM, 1978). The concept of a block size distribution of the rock mass was hinted in the ISRM Suggested Method (ISRM, 1978), recalling a similarity with the classification of soils through particle size distributions. Despite the simplicity of this concept, the adoption of a statistical approach capable of putting it into practice has not been implemented for years. The main contributions to the analytical definition of the in situ block size distribution (IBSD) are by Wang et al. (1991, 1993), Lu and Latham (1999), based on the Equation Method. First, a deterministic volume calculated from a geometrical equation involving spacing and orientation of three intersecting discontinuity planes is calculated. Then it is multiplied by tabled coefficients for assessing the IBSD. If, on one hand, this procedure is simple and feasible based on in situ survey data, on the other side, it does not allow us to consider the variability of orientation and spacing data, which is a key feature of real rock masses.

Orientation data are usually described by a Fisher distribution (Fisher, 1953; Butler, 1992; Priest, 1993):

$$P_{d\theta}(\theta) = \frac{K}{4\pi \sinh(K)} \exp\left(K \cos\theta\right) \tag{1}$$

where K is the precision parameter, called Fisher constant, and θ is the angle from the true mean. This is a symmetric distribution about the mean orientation, with a maximum at the true mean ($\theta = 0$). A large K value indicates a distribution more strongly concentrated around the true mean. Typical K values for rock joints within a set range from 20 to 300 (Kemeny and Post, 2003). The angle corresponds to the standard deviation of the normal distribution (Butler, 1992):

$$\theta = \frac{81^\circ}{\sqrt{K}} \tag{2}$$

This angle is often called the angular standard deviation or angular dispersion. For example, an angular dispersion of 30° corresponds to $K = 7.3$. Many authors (e.g. Odonne et al., 2007; Annavarapu et al., 2012) suggest using a log-normal distribution to fit discontinuity spacing data since it provides great flexibility. Gamma and Weibull's family of distributions can also be used to fit spacing data (Stavropoulou, 2014). The best distribution for a set of spacing measurements must be identified through a rigorous evaluation of the goodness of fit. The one-sample Kolmogorov–Smirnov test quantifies the distance between the empirical CDF of the sample and the theoretical CDF of the reference distribution. Therefore, it is advisable to test different distributions to create a ranking and choose the best one accordingly.

In the literature, there are two approaches to the assessment of block volume distribution: the first one is based on surveys of rock faces aiming at identifying potentially detachable blocks (Santana et al., 2012; Mavrouli et al., 2015; Mavrouli and Corominas, 2017), and the second one is based on surveys of the fallen blocks (van Veen et al., 2017; DiFrancesco et al., 2021). The distribution obtained based on the results of the geomechanical survey allows one to consider the volume as a continuous random variable. Although the range of variability may appear very widely, it is still a more reliable assessment than that based on the survey of the blocks to the slope toe. In fact, several authors have observed that the latter may be incompatible with the real one due to fragmentation, which depends strongly on the lithology and mechanical strength of the rock, as well as the presence of weak planes and not fully persistent discontinuities (Ruiz-Carulla et al., 2015, 2017; Macciotta et al., 2020; Moos et al., 2022). In highly fractured rock masses, the fallen rock blocks have a marginal role in determining block size since their volume could be affected by other processes after detachment (e.g. fragmentation). Conversely, stratigraphy and structure play a fundamental role since they mirror the degree of fracturing of the rock face. However, an accurate field observation,

i.e. the stratigraphy and structures of the rock face, is imperative for supporting any approaches to studying rockfall phenomena (Umili et al., 2020).

In consideration of the simplest case of blocks created by the intersection of three discontinuity sets K_i, K_j, and K_k, these authors propose to calculate the block volume as the product of spacings divided by a coefficient that properly considers the relative orientations among the sets:

$$V = \frac{\|\vec{\mu_i}\|\|\vec{\mu_j}\|\|\vec{\mu_k}\|}{|\sin\gamma_{ij}||\cos\delta_{k-ij}|} = \frac{S_iS_jS_k}{q} \tag{3}$$

where $\vec{\mu_i}, \vec{\mu_j}, \vec{\mu_k}$ are the director vectors of the three discontinuity sets, and therefore their norms correspond to the spacing S_i, S_j, and S_k of the three sets.

Since the circular shift of the indexes (i, j, k) is valid within the block formed by the three discontinuity planes, it is true that:

$$q = \sin\gamma_{ij}\cos\delta_{k-ij} = \sin\gamma_{jk}\cos\delta_{i-jk} = \sin\gamma_{ki}\cos\delta_{j-ki} \tag{4}$$

where γ_{ij}, γ_{jk}, γ_{ki} are the angles between pairs of sets, according to the terminology used by Palmstrøm (1996); $\delta_{k\text{-}ij}$ is the angle between the director vector $\vec{\mu_k}$ and the direction of the normal to the other two director vectors $\vec{l}_{ij}$.

The structure of this new formula is similar to that of Palmstrøm's well-known formula (Palmstrøm, 1996), with the advantage of being geometrically correct for every orientation among the three sets. Basically, q is a dimensionless number that depends only on the shape of the block, namely the angles among sets. In fact, one must consider that angles γ_{ij} among sets are limited between 0° and 180°, while $\delta_{k\text{-}ij}$ ranges between 0° and 90°: therefore, sine and cosine functions are both limited between 0 and 1. Moreover, q considers a relative orientation among the sets that physically produces a closed shape. Consequently, q ranges between 0 and 1 with a nonlinear trend. If the block is a regular prism, whose angles among sets are all equal to 90°, q is equal to 1. Fig. 1 represents the trend of q by varying K_1 orientation, while the orientation of K_2 and K_3 is kept constant. In particular, the dip of K_1 varies between 0° and 90°, the dip direction of K_1 varies between 0° and 360°, K_2 is 90/090 and K_3 is 00/000. As shown, in the cases of perpendicular sets (K_1 equal to 90/000, 90/180, and 90/360), q is equal to 1. It is worth noting that Fig. 1 reports only one of the possible trends of q. In fact, by varying the orientation of the three sets, the coefficient behaves differently: in general, the minimum and maximum values of q change (always in the range [0,1]), as well as the shape of the trend.

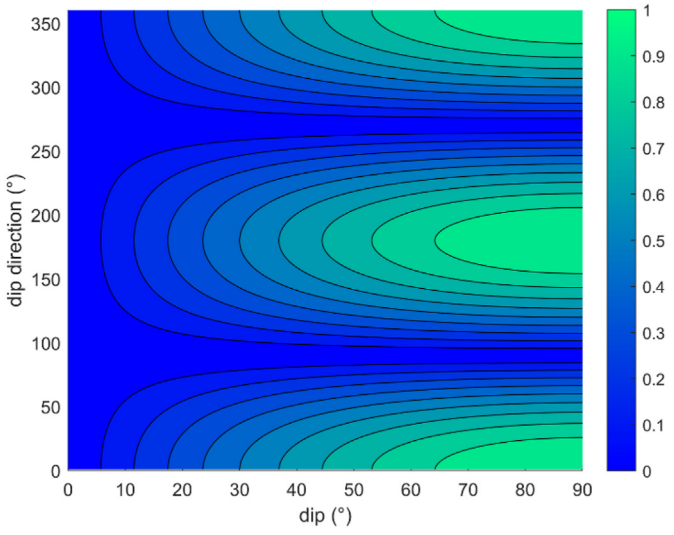

Fig. 1. Values of q by varying dip and dip direction of set K_1, while K_2 is 90/090 and K_3 is 00/000; contour step is 0.1.

It is evident that Eq. (1) is intended as a deterministic formula that requires individual values of spacing and shape factor and returns a unique value of the volume. However, a unique value of the volume is not sufficient to describe the aleatory nature of the potential blocks created by the intersection of different discontinuity sets in a rock mass.

The spacing of a discontinuity set can be considered a continuous random variable; therefore, its CDF, denoted as $F(s) = P(S \le s)$, defines the probability that a given spacing value S is less than s (Stavropoulou, 2014). The transition from the deterministic to the probabilistic approach for the IBSD analytical assessment is possible by assuming that the spacing distributions of the three discontinuity sets are independent. Therefore, the CDF of the product of the three spacings can be written as

$$F_{S_1S_2S_3}(s_1, s_2, s_3) = P(S_1 \le s_1, S_2 \le s_2, S_3 \le s_3) \tag{5}$$

Then, it is simply the product of their CDF:

$$F_{S_1S_2S_3}(s_1, s_2, s_3) = F_{S_1}(s_1)F_{S_2}(s_2)F_{S_3}(s_3) \tag{6}$$

In terms of probability, this corresponds to:

$$P(S_1 = s_1, S_2 = s_2, S_3 = s_3) = P(S_1 = s_1)P(S_2 = s_2)P(S_3 = s_3) \tag{7}$$

Therefore, considering Eq. (3) proposed by these authors and assuming q as a constant, the CDF of the block volume can be written as

$$F_V(v) = \frac{F_{S_1}(s_1)F_{S_2}(s_2)F_{S_3}(s_3)}{q} \tag{8}$$

It represents the analytical definition of the IBSD based on the correct geometrical equation for calculating block volume. The assumption of a constant value of q while changing the spacing values neglects the effect of orientation variability. While this is a simplification of the problem, it has been observed that uncertainty in spacing values amplifies block volume uncertainty in a more significant way than that of orientation (Ferrero et al., 2015). The variance of a random variable can express its uncertainty, since it is a measure of its dispersion. Therefore, since both spacing and volume can be considered continuous random variables, the influence of the uncertainty related to input spacing values can be quantified and associated with the output volume values.

Based on Eqs. (3) and (8), it is possible to calculate the volume expected value $E[V]$ and variance $\mathrm{Var}[V]$ based on the spacing expected value $E[S]$ and variance $\mathrm{Var}[S]$ of the three sets. Considering only the numerator of Eq. (8) under the hypotheses that:

(1) Spacing S_i of a generic ith discontinuity set is a continuous random variable, whose $E[S]$ and $\mathrm{Var}[S]$ are μ_i and σ_i^2, respectively;
(2) Spacing S_i and S_j of two different discontinuity sets are independent, therefore their covariance $\mathrm{Cov}[S_i, S_j] = 0$. This hypothesis corresponds to the most general case of discontinuity planes belonging to a set, whose location in a rock mass is independent of the location of planes belonging to a different set.

It is possible to calculate the expected value and the variance of the product of spacing S_1 and S_2 by (Baecher and Christian, 2003)

$$E[S_1S_2] = \mu_1\mu_2 \tag{9}$$

$$Var[S_1S_2] = \mu_1^2\sigma_2^2 + \mu_2^2\sigma_1^2 + \sigma_1^2\sigma_2^2 \tag{10}$$

By extension, it is possible to calculate the expected value and the variance of the product of spacing S_1, S_2, and S_3 as follows:

$$E[S_1S_2S_3] = \mu_1\mu_2\mu_3 \tag{11}$$

$$Var[S_1S_2S_3] = (E[S_1S_2])^2\sigma_3^2 + \mu_3^2 Var[S_1S_2] + Var[S_1S_2]\sigma_3^2 \tag{12}$$

By replacing Eqs. (9) and (10) in Eq. (12), we have

$$Var[S_1S_2S_3] = \mu_1^2\mu_2^2\sigma_3^2 + \mu_1^2\mu_3^2\sigma_2^2 + \mu_2^2\mu_3^2\sigma_1^2 + \mu_3^2\sigma_1^2\sigma_2^2 + \mu_1^2\sigma_2^2\sigma_3^2 + \mu_2^2\sigma_1^2\sigma_3^2 + \sigma_1^2\sigma_2^2\sigma_3^2 \tag{13}$$

Based on Eqs. (3), (11) and (13), under the assumption of constant q ($E[q] = q$, $Var[q] = 0$), it is possible to explicitly calculate the expected value and variance of the volume as follows:

$$E[V] = \frac{\mu_1\mu_2\mu_3}{q} \tag{14}$$

$$Var[V] = \mu_1^2\mu_2^2\sigma_3^2 + \mu_1^2\mu_3^2\sigma_2^2 + \mu_2^2\mu_3^2\sigma_1^2 + \mu_3^2\sigma_1^2\sigma_2^2 + \mu_1^2\sigma_2^2\sigma_3^2 + \mu_2^2\sigma_1^2\sigma_3^2 + \sigma_1^2\sigma_2^2\sigma_3^2 \tag{15}$$

Eq. (14) provides an average value of the volume, while Eq. (15) provides the variance of the volume, considering the combined effects of spacings variability, both in terms of mean and variance.

2.2. Block shape

The shape of blocks can vary significantly within a rock mass. Regular geometric shapes are the exception rather than the rule since the joints in any one set are seldom consistently parallel (ISRM, 1978). Palmstrøm (1995) introduced a shape factor β to quantify the equivalent block volume for rock masses with few joint sets. There are two similar definitions of this shape factor, but in any case, the variables are the longest and shortest dimensions of the block. Palmstrøm (2001) also provided a diagram for the classification of the block shape as a function of the ratio of the longest edge (*Lo*) of the block over the shortest one (*Sh*), versus the ratio of the intermediate edge (*In*) over *Sh*. In this logarithmic diagram (Fig. 2), blocks can be classified as:

(1) Equidimensional or compact prisms, with $In/Sh < 2$ and $Lo/Sh < 2$;
(2) Long prisms (rods), with $In/Sh < 2$ and $Lo/Sh > 2$;
(3) Long flat prisms (blades), with $2 < In/Sh < 1+(Lo/Sh - 1)^{0.5}$; and
(4) Flat prisms (slabs), $In/Sh > 1+(Lo/Sh - 1)^{0.5}$.

Another approach to relate a single block or a compartment of the rock mass to its volume through a shape factor was proposed by Hantz (2011). In a general formulation, the relationship between the volume (V) and the width (w) of the fallen compartments may be written as $V = kw^3$, where k is a shape factor, which equals 0.5 for the calcareous cliffs of the Grenoble area. However, the k factor can range between 0.4 and 2. If k is unknown, the author recommends using the value of 1. This simplified approach could be helpful in back analyses of rockfall phenomena for attributing a probability of not being exceeded to the actual detached volume.

Other authors employed discrete fracture network (DFN) generators to create more complex and accurate descriptions of the block shape, as in the case of Kalenchuk et al. (2006, 2008). These authors introduced a pair of a dimensional parameters (α and β) to be used in a triangular diagram to describe the geometry of the rock blocks. The parameter α is defined as a function of the volume, surface area, and average edge length, while β is a function of the length of the longest and shortest edges of the block. In the case of prismatic blocks, as in almost every possible natural scenario, both α and β have a maximum value of 10. Both parameters are used to define a triangular chart, similar to the diagram in Palmstrøm (2001). In this case, the area of the diagram is divided into sectors with which a specific shape is associated (Fig. 2). The authors of these studies also noted a relationship between the size of the block and its shape: in general, the larger the volume, the less variable the shape. The principal limitation of this approach lies in the fact that

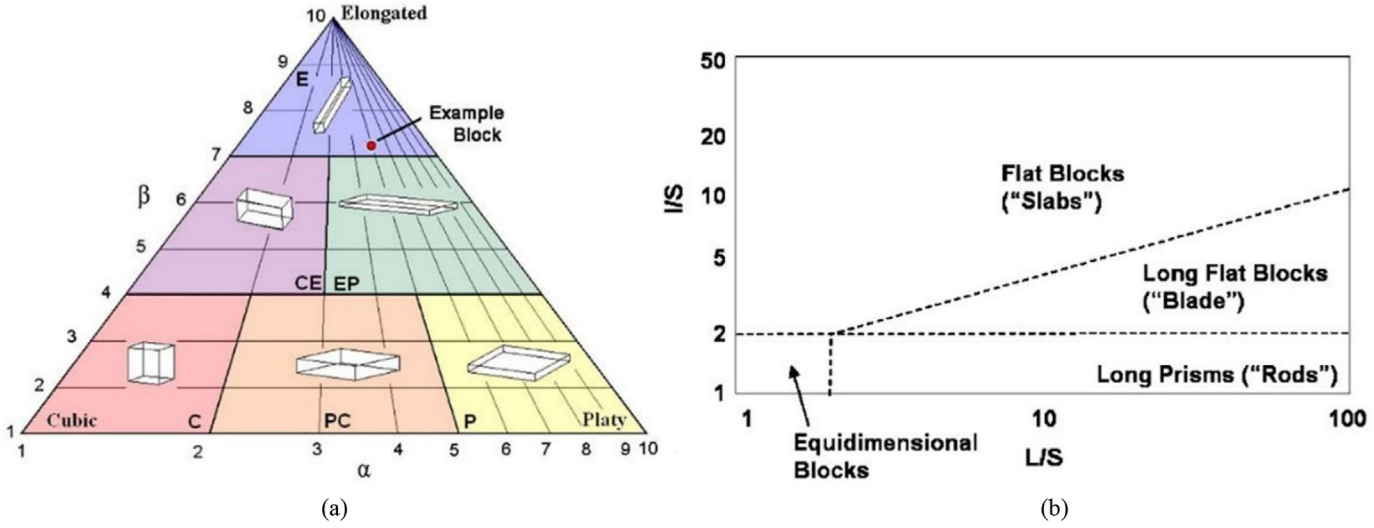

Fig. 2. (a) Shape classification triangular diagram proposed by Kalenchuk et al. (2006, 2008), and (b) Shape classification diagram proposed by Palmstrøm (2001).

calculating α and β requires knowing the coordinates of every vertex of all the blocks in the considered rock mass, which is a relatively simple task only when employing DFN software.

3. Calculation

3.1. Case study

A fictitious rock face and the slope underneath were considered as the case study. This choice was dictated by the need to have complete control over the variables to assess the effects of the uncertainties quantitatively. Three perpendicular discontinuity sets, K_1, K_2, and K_3 were assumed to be surveyed in the rock face. For each discontinuity set, the distribution of spacing values was assigned, while orientation dispersion was considered null within each set, consistent with the assumption of constant q made for defining Eq. (8); in this case, q is equal to 1.

A digital terrain model (DTM) describing a real slope was used for this study. The test area is morphologically quite simple, with an upper portion characterized by a quasi-regular surface that transitions to a system of gullies and, lastly, to a deep incision. The slope was chosen with the help of a geomorphologist to avoid local or improbable effects on the expected trajectories. In this way, it was possible to appreciate the effect of block size and shape both on a regular surface and where the morphology has a more prominent influence. The DTM employed is freely provided by the regional authorities (Regione Piemonte, 2011) in GeoTIFF format, with a pixel size of 5 m × 5 m and a vertical resolution of approximately 0.5 m. The slope is 2450 m long and the source area is 1475 m wide, with an elevation difference from the top to the toe of 1000 m. The slope length allows us to visualize the difference in terms of energy and runout distance produced by different block volumes and shapes. The average slope angle is only 22°, but locally this value increases up to 70°. It was assumed that all the slope is made up of the same material, while the source area, located close to the uppermost border of the slope, was defined by a 20 m wide band that crosses almost the entire slope. The choice of not completely covering the slope was made to avoid miscalculations near the boundaries of the DTM. Rockyfor3D software (Dorren, 2016) was chosen for performing the simulations of trajectories of single, individually falling rocks, in three dimensions. In this study, the characteristics and features of the slope were kept as simple as possible. All the parameters required by the software, such as surface asperities, soil type, or vegetation, have been set for all the simulations to the same values, with reference to those provided by Dorren (2016). In this way, it was possible to assess the effect of block shape on the simulated trajectories while the interference of all the other parameters related to the slope was kept at constant. For this, a soil type corresponding to medium compact soil with small rock fragments ($d < 0.1$ m) was chosen, having a normal restitution coefficient (R_n) with a range of 0.3–0.36 and an average value of 0.33. At the lowest positions of the DTM, a small band of water has been modeled so that any block reaching it would be stopped, and its propagation would not continue outside the DTM itself. Lastly, all the parameters describing the vegetation have been ignored, and their effects have been set to null. The slope is visible in Fig. 3.

3.2. IBSD and related uncertainties

The spacing distribution was set to behave as a Gamma distribution; moreover, the same Gamma distribution was assumed for the three discontinuity sets. It is useful to recall that the Gamma distribution is a continuous probability distribution described by two parameters: a shape parameter a and a scale parameter b. Its PDF can be expressed as

$$f(x) = \frac{1}{b^a \Gamma(a)} x^{a-1} e^{\frac{-x}{b}} \tag{16}$$

The mean and variance can be calculated as

$$\mu = ab \tag{17}$$

$$\sigma^2 = ab^2 \tag{18}$$

In order to assess the influence of the spacing uncertainty on the volume CDF, μ was considered equal to 1 m, while σ^2 varied from 10^{-6} to 0.49. A total of 9 spacing PDFs was generated (Fig. 4), and assumed as a reasonable approximation (Table 1). Fig. 5 shows the corresponding CDFs: the larger the variance, the wider the range of possible spacing values. It is also worth noting that the spacing value with a cumulative frequency equal to 50%, in general, is not equal to μ.

Samples consisting of different numbers of spacing values ($N = 100$ or 50) were then extracted from the true population by inverting each true PDF in correspondence with N randomly generated values from the uniform distribution in the interval (0, 1). Then, the samples were fitted by a Gamma distribution, and the two parameters (a, b) were estimated. In Table 1, the estimated μ

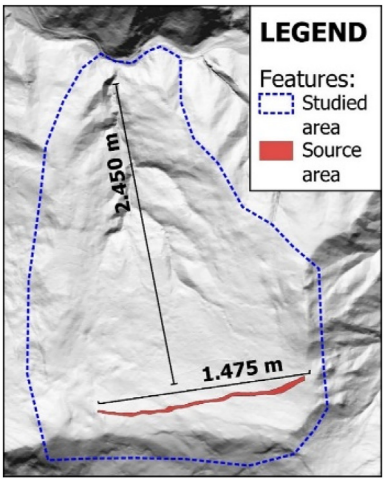

Fig. 3. Slope used for simulations, with the indication of the source area.

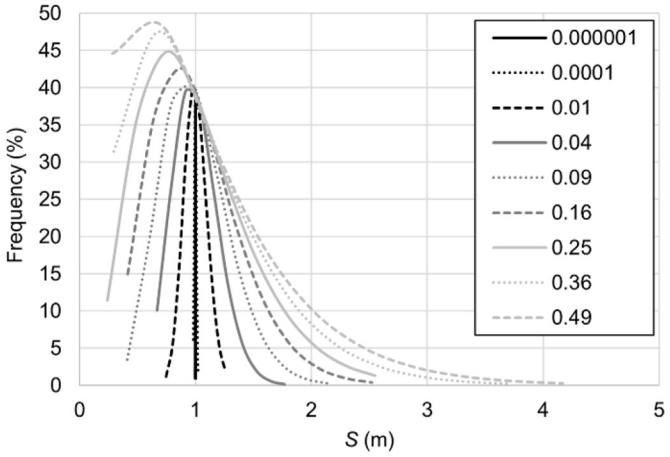

Fig. 4. True spacing PDFs (values of σ^2 in Table 1).

Table 1
Summary of the synthetic spacing PDFs (constant μ, 9 values of σ^2) and the corresponding best fitting Gamma PDFs, considering 2 different values of N.

True PDF		$N = 100$		$N = 50$	
Assigned μ (m)	Assigned Σ^2 (m^2)	Eq. (17) M (m)	Eq. (18) σ^2 (m^2)	Eq. (17) M (m)	Eq. (18) σ^2 (m^2)
1	1×10^{-6}	1	1.16×10^{-6}	1	1.09×10^{-6}
1	1×10^{-4}	1	1.06×10^{-4}	0.99	1.05×10^{-4}
1	0.01	0.99	0.012	0.97	0.011
1	0.04	0.99	0.041	0.95	0.049
1	0.09	0.99	0.094	1.07	0.106
1	0.16	0.96	0.125	0.99	0.159
1	0.25	1.06	0.271	0.91	0.178
1	0.36	0.87	0.283	0.98	0.414
1	0.49	0.98	0.501	0.94	0.328

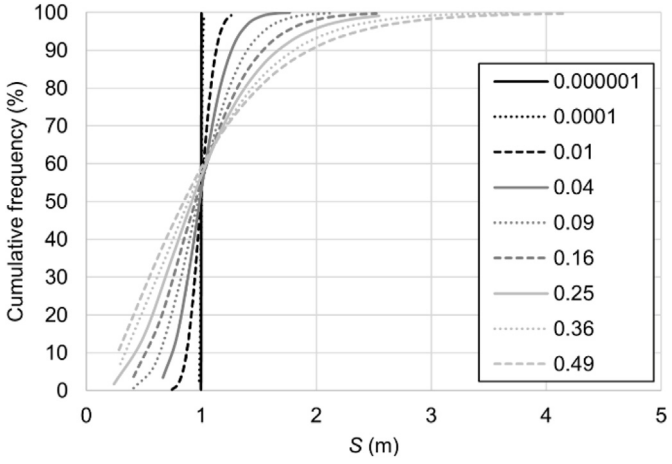

Fig. 5. True spacing CDFs generated from true PDFs (Fig. 4).

and σ^2 (Eq. (17) and (18)) of the fitted PDFs are compared with the true ones. As expected, a decrease in N leads to a general increase in the difference between the estimated μ and the true one. The same effect, which is also amplified by the rise of the true σ^2, can be observed on the estimated σ^2.

$E[V]$ and $\mathrm{Var}[V]$ can be estimated from Eqs (14) and (15). For the case study considered, equal mean spacing $\mu_1 = \mu_2 = \mu_3 = \mu$, equal variance $\sigma_1^2 = \sigma_2^2 = \sigma_3^2 = \sigma^2$, and $q = 1$ are assumed. Therefore, Eqs. (14) and (15) can be reduced as follows:

$$\mathrm{E}[V] = \mu^3 \tag{19}$$

$$\mathrm{Var}[V] = 3\mu^4\sigma^2 + 3\mu^2\sigma^4 + \sigma^6 \tag{20}$$

In the special case of unit mean spacing $\mu_1 = \mu_2 = \mu_3 = \mu = 1$ Eqs. (19) and (20) can be further reduced as

$$E[V] = 1 \tag{21}$$

$$\mathrm{Var}[V] = 3\sigma^2 + 3\sigma^4 + \sigma^6 \tag{22}$$

Fig. 6 shows $\mathrm{Var}[V]$, calculated with Eq. (20), as a function of σ^2, considering different values of μ. One can observe that $\mathrm{Var}[V]$ increases by some order of magnitude by increasing σ^2: this effect is wider for smaller values of μ.

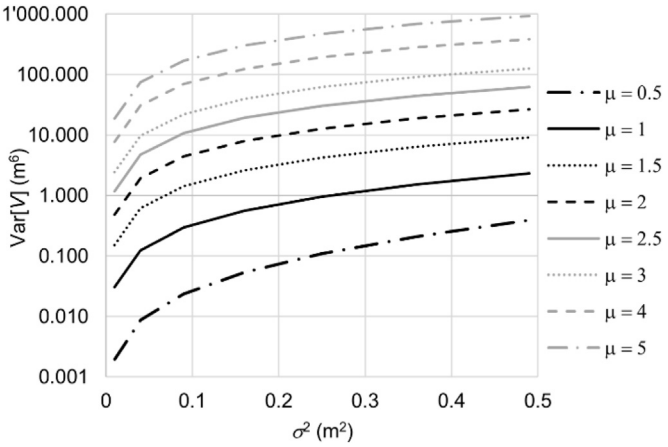

Fig. 6. $\mathrm{Var}[V]$ (Eq. (20)) as a function of σ^2, considering different values of μ. [μ should be in italic type].

3.3. Block shape and related uncertainties

The most common approach to block shape consists of definition a reference shape, which is usually considered as the most frequent shape associated with fallen blocks or measurable in the rock mass itself using the methods described in Section 2.2. It is also often assumed that this reference shape is a constant feature related to every block size. However, there is evidence in the literature that this is not the case. For example, Kalenchuk et al. (2006, 2008) produced a chart in which the size of the blocks, measured through a DFN, is plotted against the shape. These diagrams show that shape is anything but constant and has a relationship with block size.

If we consider a block of prismatic shape where all the sides are orthogonal to each other, $q = 1$, and the length of the sides corresponds to the spacings of the three joint sets generating the block, which are assumed to be known. Then, the block, whose volume corresponds to $E[V]$ calculated with Eq. (14), can be plotted on the shape classification diagram provided by Palmstrøm (2001). By iterating the process for every value in the range covered by the volume CDF, we can map all the possible shapes assumed by the blocks. It is, therefore, possible to assess the variation by quantifying the relative frequency of each shape in a given volume CDF. It is also possible to observe any relationship between the shape and size of the block, which would appear as a degree of organization in the shape diagram. For example, in the simplest case, one could observe that for larger volumes, the shape tends to fall in a specific portion of the graph. Lastly, this approach also allows us to visualize that an assigned reference shape does not represent the entire volume CDF.

3.4. Simulation of block trajectories

Two sets of numerical simulations were carried out using the software Rockyfor3D (Dorren, 2016) to compute the trajectories and visualize the effect of uncertainties on block volume and shape. This software was chosen because of its ability to account for the shape of the simulated block. Although only simple shapes can be assumed in the simulations, this is sufficient to assess the influence of block shape on the trajectories. The software considers a significant number of parameters, such as the block volume, block shape, slope, and source areas or points. To describe each of these features, Rockyfor3D employs raster maps in ASCII format, easily obtainable using any geographic information system (GIS). The

raster files can describe the analyzed problem in detail, considering that up to fourteen different parameters can be considered.

The shape of the simulated block is defined using four parameters: a block shape number and three main diameters (d_1, d_2, and d_3). The block shape number defines the family of shapes the block belongs to, which directly translates into the formula used to calculate the associated volume. In this study, the block was always assumed to have a regular shape and was treated as an orthogonal prism. Here, the d_1, d_2, and d_3 values correspond to the mean spacing of the three joint sets, given the orthogonal configuration of the block shape. The volume of the block is therefore calculated as

$$V = d_1 d_2 d_3 = \mu_1 \mu_2 \mu_3 \tag{23}$$

Table 2
$E[V]$ and Var$[V]$ calculated with Eqs. (21) and (22) for the spacing distributions in Table 1.

True PDF		$N = 100$		$N = 50$	
Eq. (21) $E[V]$ (m^3)	Eq. (22) Var$[V]$ (m^6)	Eq. (21) $E[V]$ (m^3)	Eq. (22) Var$[V]$ (m^6)	Eq. (21) $E[V]$ (m^3)	Eq. (22) Var$[V]$ (m^6)
1	3×10^{-6}	1	3.5×10^{-6}	1	3.3×10^{-6}
1	3×10^{-4}	1	3.2×10^{-4}	0.99	3.1×10^{-4}
1	0.03	0.98	0.03	0.91	0.03
1	0.12	0.97	0.12	0.85	0.12
1	0.3	0.98	0.3	1.21	0.45
1	0.56	0.89	0.37	0.97	0.54
1	0.95	1.2	1.3	0.75	0.45
1	1.52	0.65	0.68	0.93	1.69
1	2.31	0.95	2.25	0.82	1.07

Table 3
$E[V]$ and Var$[V]$ estimated from the Monte Carlo simulations performed for the spacing distributions in Table 1.

True PDF		$N = 100$		$N = 50$	
$E[V]$ (m^3)	Var$[V]$ (m^6)	$E[V]$ (m^3)	Var$[V]$ (m^6)	$E[V]$ (m^3)	Var$[V]$ (m^6)
1	3.23×10^{-6}	1	3.23×10^{-6}	1	2.85×10^{-6}
1	3.24×10^{-4}	1	2.98×10^{-4}	1	2.23×10^{-4}
1.01	0.03	1.05	0.03	1	0.03
1.02	0.14	0.92	0.1	1.09	0.15
1.03	0.34	1.09	0.28	0.91	0.22
1.05	0.67	1.01	0.55	1.06	0.71
1.06	1.21	0.96	1.23	0.68	0.46
1.08	2.07	1.35	2.29	1	1.5
1.1	3.46	1.17	3.63	1.26	3.27

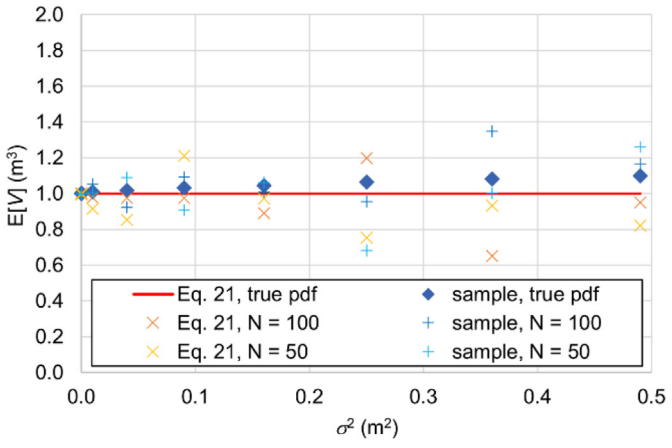

Fig. 7. $E[V]$ as a function of σ^2 (Eq. (21)).

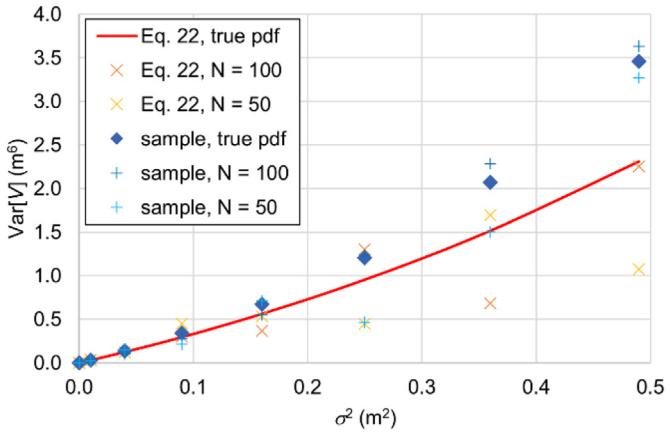

Fig. 8. Var$[V]$ as a function of σ^2.

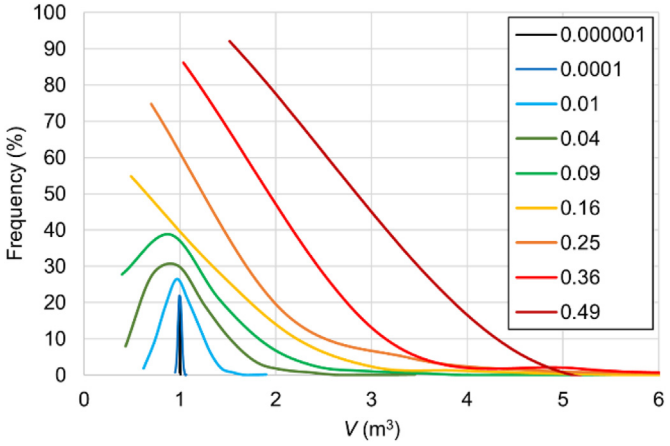

Fig. 9. Volume PDFs generated from synthetic distributions in Table 1 for different values of σ^2.

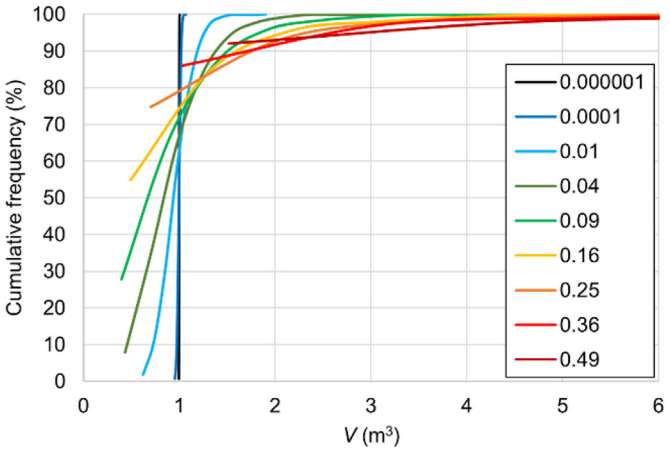

Fig. 10. Volume CDFs generated from synthetic distributions in Table 1 for different values of σ^2.

The density considered in this study is 2700 kg/m^3, roughly equivalent to that of limestone.

Table 4
Input parameters to describe the spacing and volume CDFs for the expected cubic and prismatic block shapes.

Expected Shape	Spacing						Volume			
	K_1		K_2		K_3		Eq. (14)	Eq. (15)	Sample	
	μ_1 (m)	σ_1^2 (m^2)	μ_2 (m)	σ_2^2 (m^2)	μ_3 (m)	σ_3^2 (m^2)	$E[V]$ (m^3)	Var[V] (m^6)	$E[V]$ (m^3)	Var[V] (m^6)
Cube	1.71	0.25	1.71	0.25	1.71	0.25	5	6.98	4.91	6.46
Prism	1	0.25	2	0.25	2.5	0.25	5	9.53	5.01	10.68

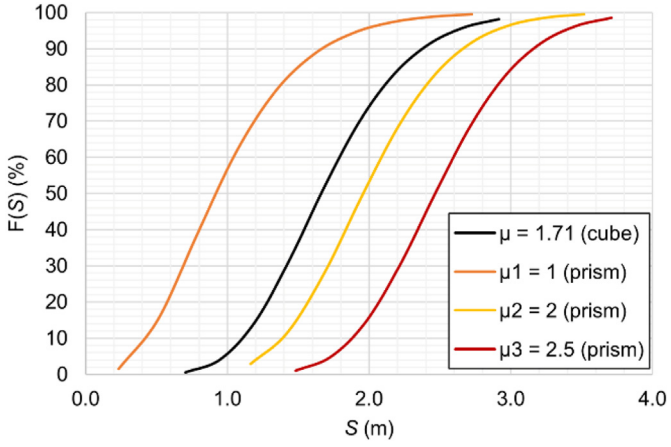

Fig. 11. Spacing CDFs (Table 4).

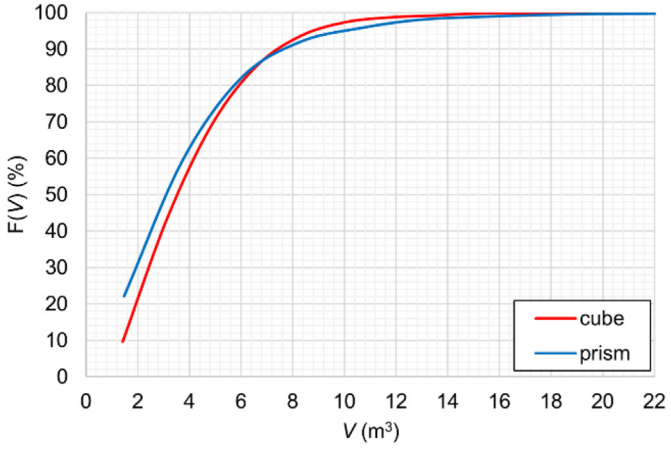

Fig. 12. Volume CDFs (Table 4).

4. Results and discussion

4.1. IBSD construction

Based on the spacing distributions in Table 1, $E[V]$ and Var[V] can be calculated with Eqs. (21) and (22) proposed by these authors, without the need to generate the volume CDF. In detail, the values of μ and σ^2 in the first and second columns of Table 1 were used to calculate $E[V]$ and Var[V] reported in the first and second columns of Table 2. The same process was carried out for the columns regarding $N = 100$ and $N = 50$.

To demonstrate the validity of Eqs. (21) and (22), the volume samples were generated through Monte Carlo simulations based on spacing distributions in Table 1. Eq. (8) was used to calculate the volume. Consistent with the assumptions made for deriving Eqs. (21) and (22), the same spacing distribution, with a unit mean spacing, was assumed for all three discontinuity sets from which the blocks originate. $E[V]$ and Var[V] of the volume samples were calculated (see Table 3) and compared with those assessed with Eqs. (21) and (22) (see Table 2). Figs. 7 and 8 show the comparison between values in Tables 2 and 3 in terms of $E[V]$ and Var[V], respectively. The first remark is that $E[V]$ and Var[V] calculated for the sample generated from the true distribution tend to gradually diverge from the ones calculated with Eqs. (21) and (22), due to the increasing of σ^2. This fact can also be observed in the $E[V]$ and Var[V] calculated with Eqs. (21) and (22) and from the samples, but the values do not show a clear increasing trend: the combined variation of μ and σ^2 from the true ones, considered three times (corresponding to the three discontinuity sets), does not produce a direct proportionality in the increase of $E[V]$ and Var[V]. In general, the comparison shows a good agreement of the results, making the proposed equations suitable for being used as estimators of $E[V]$ and Var[V] given μ and σ^2 from in situ surveys.

The obtained volume PDFs and CDFs generated from synthetic distributions in Table 1 are shown in Figs. 9 and 10, respectively. The larger the σ^2, the wider the range of possible volume values. This visually corresponds to a tendency towards an almost horizontal CDF for increasing σ^2. It is also worth noting that volume value with a cumulative frequency equal to 50% generally is not equal to $E[V]$.

4.2. Shape assessment

Based on the considerations in Section 3.3, two cases were analyzed to highlight the importance of proper block shape assessment: the first considers three coincident spacing distributions to produce a cubic expected shape, while the second considers three different spacing distributions to create a prismatic

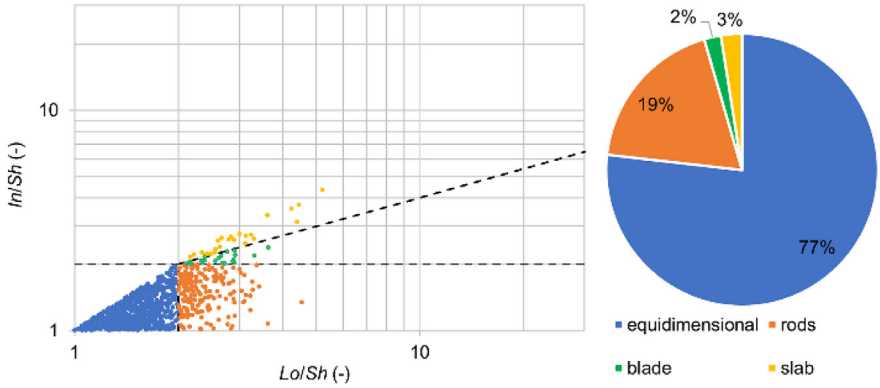

Fig. 13. Shape distribution for the cubic expected shape.

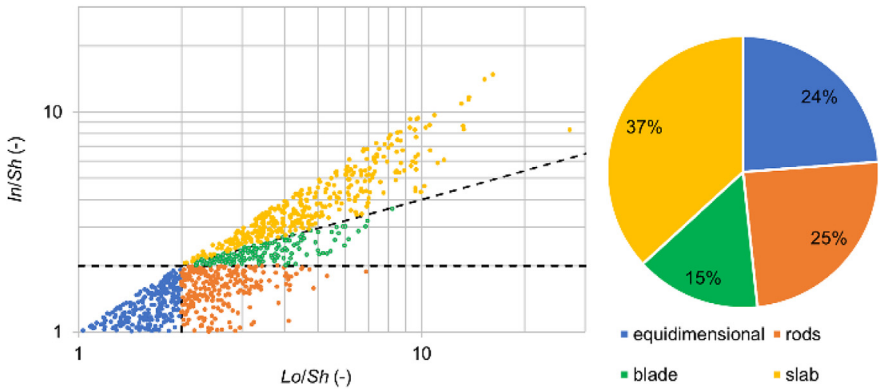

Fig. 14. Shape distribution for the prismatic expected shape.

expected shape. Table 4 reports the parameters describing the input data for the two cases: they are characterized by equal $E[V]$ and σ^2 but different values of μ. Spacing samples were then extracted from the true population by inverting each true distribution in correspondence with 1000 randomly generated values from the uniform distribution in the interval (0, 1). The volume sample (1000 data) was obtained by multiplying each triplet of spacing values. Eqs. (14) and (15) were applied to calculate $E[V]$ and Var[V] and compare the results with those estimated from the volume sample. The good agreement among the results confirms the validity of the proposed equations and the method in general. Spacing CDFs and volume CDFs are shown in Figs. 11 and 12, respectively. The spacing samples relative to the cubic expected shape were processed to calculate the *Lo/Sh* and *In/Sh* ratios. The obtained values were plotted on the shape diagram (Fig. 13) and classified. The equidimensional type is indeed predominant (77%), but the rod shape is well represented (19%) too. The same process was performed considering the spacing samples relative to the prismatic expected shape (Fig. 14). In this case, the distribution of the shape types is more balanced, with a predominance of slabs (37%).

Lastly, Figs. 15 and 16 illustrate the effect of block size over block shape for the same two cases considered above. In the cubic case, an increase in volume does not produce a clear impact on the block

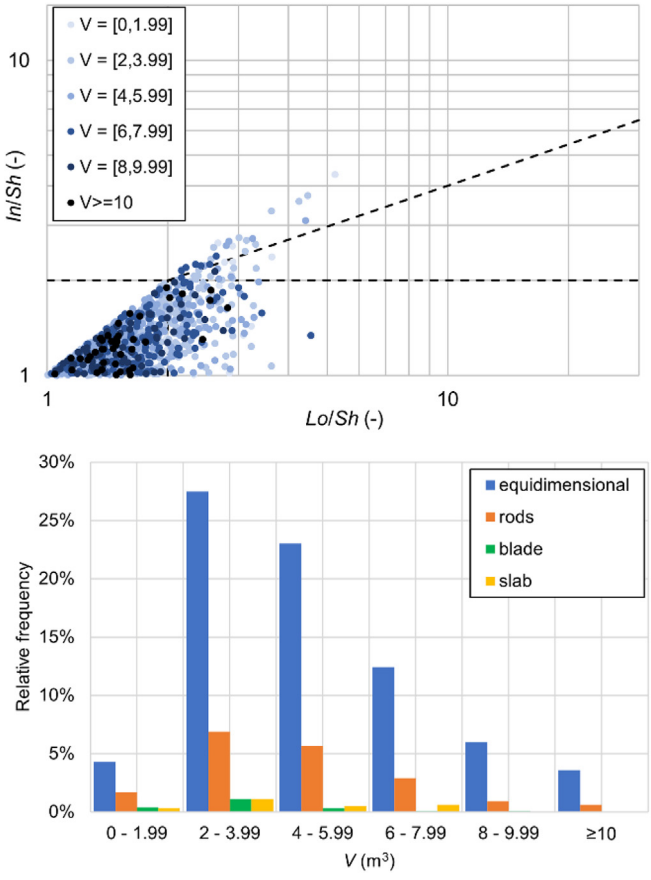

Fig. 15. Shape distribution with respect to block size (V) for the cubic expected shape.

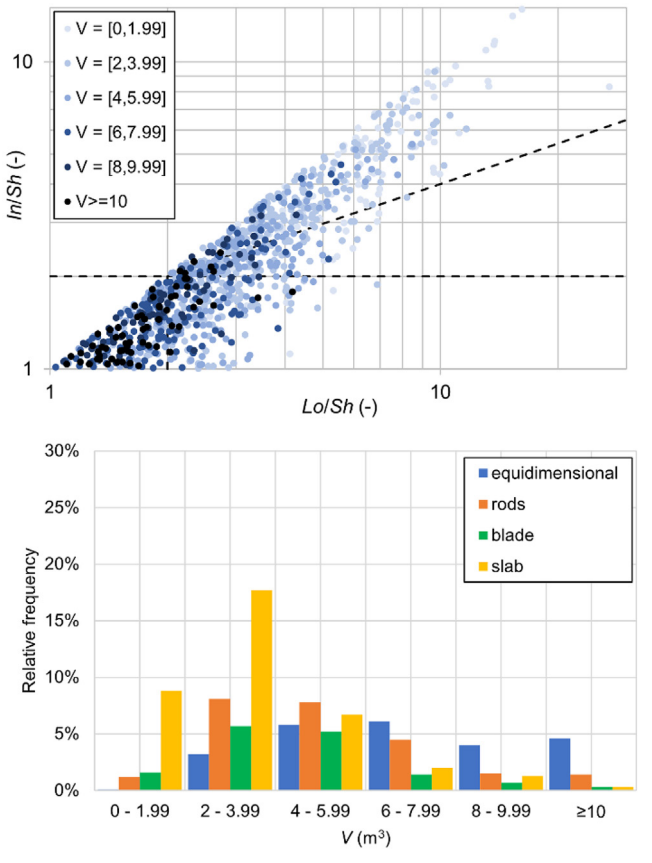

Fig. 16. Shape distribution with respect to block size (V) for the prismatic expected shape.

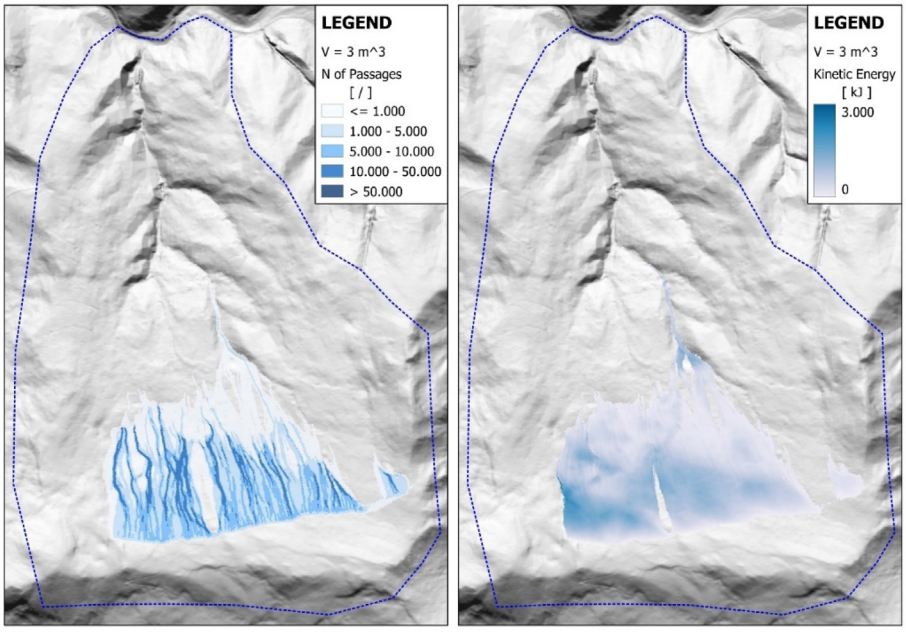

Fig. 17. (a) Trajectories and runout, and (b) Maximum kinetic energy of the 3 m^3 cubic block.

Table 5
Geometrical features and classification parameters of the five shapes considered in the simulations.

ID	*Sh* (m)	*In* (m)	*Lo* (m)	*V* (m^3)	*Lo*/*Sh*	*In*/*Sh*
B1	1.71	1.71	1.71	5	1.1	1.1
B2	0.77	0.85	7.69	5	10	1.1
B3	0.64	1.61	4.83	5	7.5	2.5
B4	0.58	2.92	2.92	5	5	5
B5	1.08	2.15	2.15	5	2	2

shape, and this is distributed independently across the diagram. In the case of the prismatic expected block, however, a global trend exists, associating larger volumes with more equidimensional shapes. This confirms what was observed by Kalenchuk et al. (2006, 2008) and highlights the effect of the different spacing CDFs.

These analyses support the importance of carrying out Monte Carlo simulations to have an overall view of the case and make assumptions about block shape that can be quantitatively associated with a probability of occurrence.

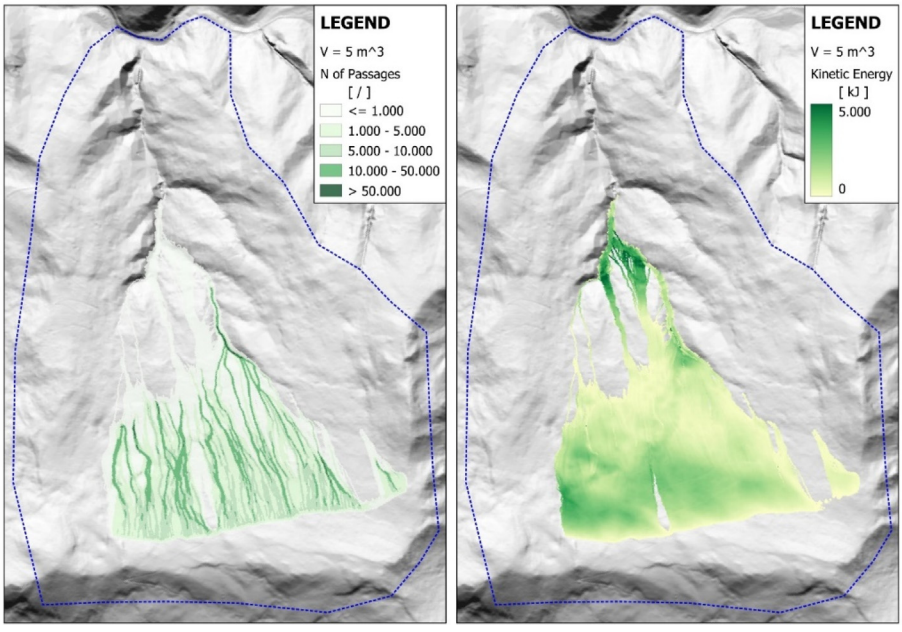

Fig. 18. (a) Trajectories and runout and (b) Maximum kinetic energy of the 5 m^3 cubic block.

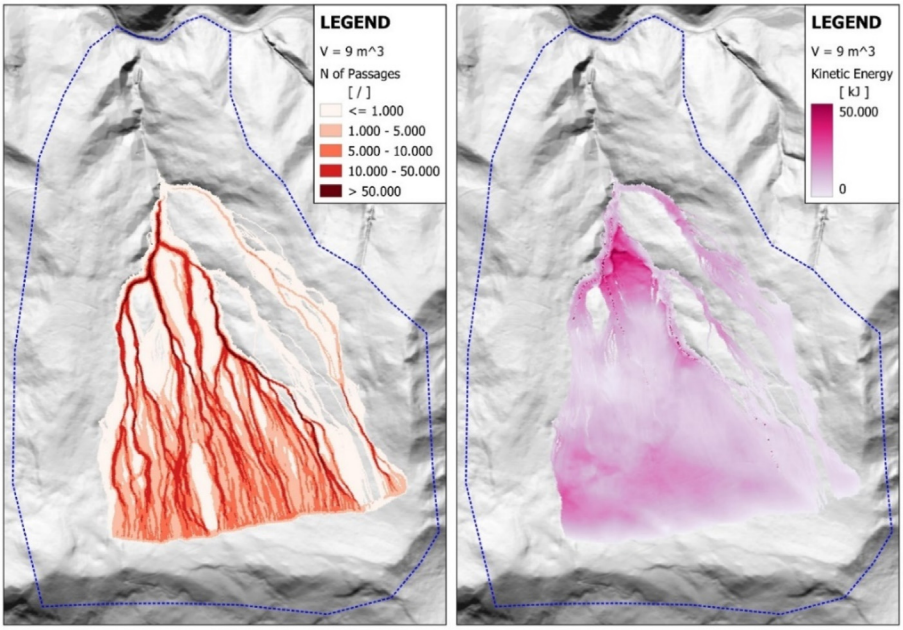

(a) (b)

Fig. 19. (a) Trajectories and runout and (b) Maximum kinetic energy of the 9 m^3 cubic block.

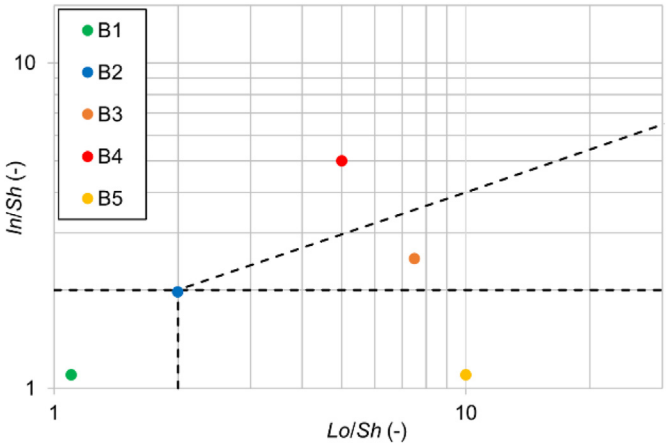

Fig. 20. The five block shapes considered in the second set of numerical simulations, plotted on the classification diagram proposed by Palmstrøm (2001).

4.3. Effect of the uncertainties on block trajectories

Two sets of numerical simulations were performed to assess the effect of block size and shape on the dynamic of rockfall phenomena. For the first set of simulations, the block shape was kept constant (cubic or equidimensional), while the volume of the simulated block was varied by changing the parameter d_1 (where $d_1 = d_2 = d_3$). Specifically, blocks with volumes of 3 m^3, 5 m^3, and 9 m^3 were considered. These values were chosen on the CDF of cubic blocks in Fig. 12 and correspond to a cumulative frequency of 40%, 70%, and 96%, respectively. The simulations considered the entire source area releasing blocks of constant volume. As expected, volume change influences the runout of the simulated phenomena and the energies involved. The simulations are portrayed in Figs. 17–19, where both runout trajectories and kinetic energy are shown for each of the three cases.

As can be seen, an increase in volume results in longer runouts and significantly higher kinetic energy. The runout of the 3 m^3 block barely reaches the first gully in the middle section of the slope, while both the 5 m^3 and the 9 m^3 blocks reach the lower portion of the slope. It should also be noted the effect of morphology is less significant at higher block volumes, especially in the upper part of the slope. In terms of the amount of energy involved in the phenomenon, the 3 m^3 and the 5 m^3 blocks have a similar level of kinetic energy, while the 9 m^3 block involves energies one order of magnitude higher. Similarly, the kinetic energy distribution along the slope is comparable for the 3 m^3 and the 5 m^3 blocks, where the highest energies were recorded in the upper part of the slope, just below the source area, and in the gullies in the middle sector of the slope. For the 9 m^3 block, the highest energy levels were found in the lower portion of the slope, where the morphology of the test slope forces the trajectories to converge in the main gully (see Fig. 19).

The second set of simulations was performed to visualize the difference produced by the shape of the block, while keeping the volume constant. In particular, the volume was set equal to 5 m^3, and the output trajectories obtained previously for the cubic block (Fig. 17) were used as a reference (B1 in Table 5). Three different test block shapes (B3, B4, B5) were assumed, as described in Table 5 and plotted on the diagram provided by Palmstrøm (2001) (see Fig. 20), so that each of the other shape categories (rod-like, blade-like, and slab-like) was represented. The special case described by the intersection of the boundaries of the different sectors was also considered and modeled (B2). The effect of shape is portrayed in Figs. 21 and 22, where one can appreciate a significant change in runout distance and trajectories.

As can be observed, the difference between the reference cubic block and the other shapes is substantial: the runout increases significantly, and the way the trajectories concentrate varies for the different shapes. The blade-like block (Case B3) is the one that manifests the more widespread trajectories, while the rod-like block (Case B5) shows a tendency towards concentration on the left side of the slope. Conversely, the slab-like block (B4) shows a

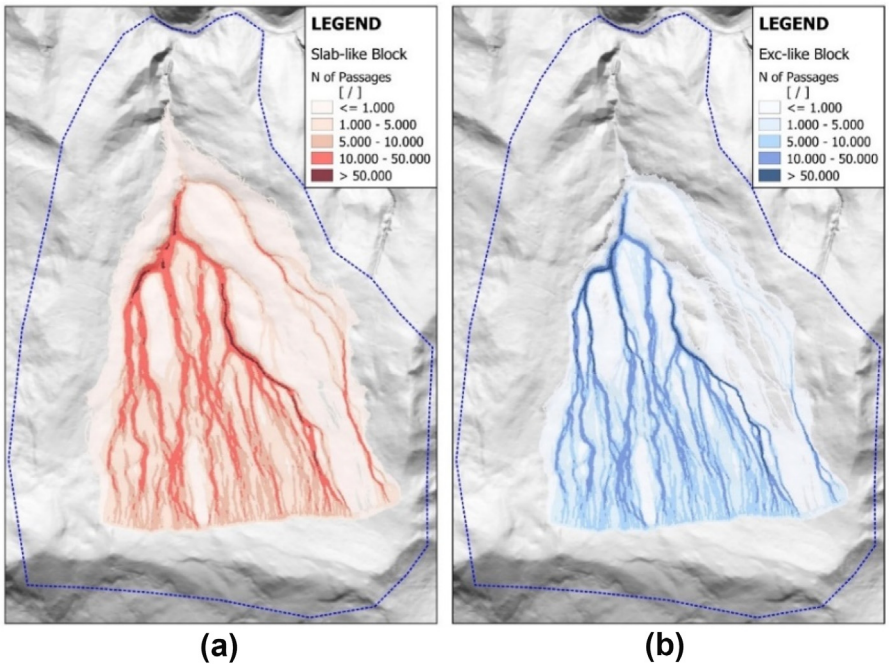

Fig. 21. Trajectories of the simulated: (a) Slab-like block B4, and (b) Special case B2.

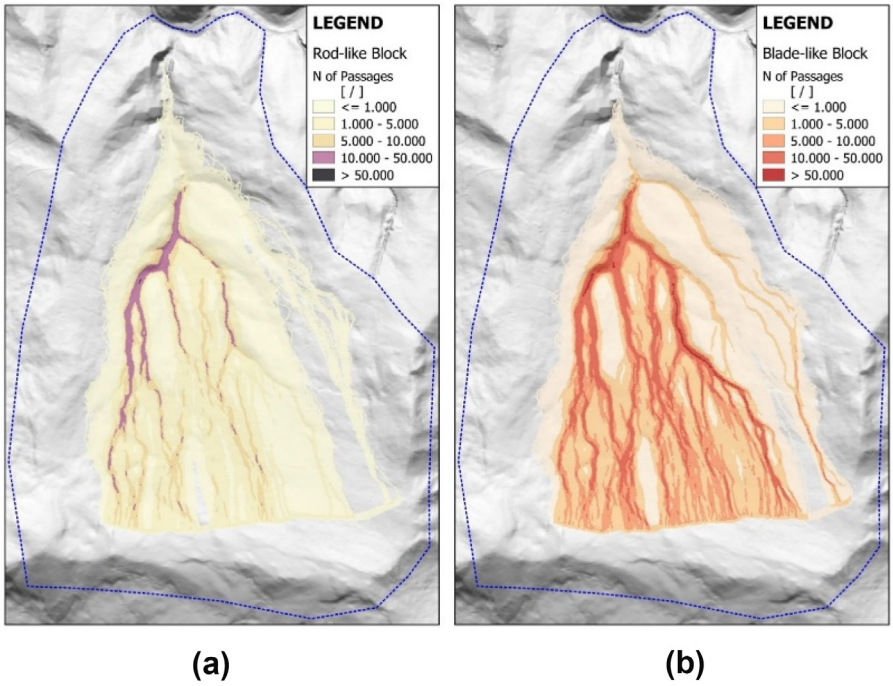

Fig. 22. Trajectories of the simulated: (a) Rod-like block B5, and (b) Blade-like block B3.

Table 6
Some practical examples of uncertainty effect assessment.

Expected Shape	Spacing						Volume			
	K_1		K_2		K_3		Eq. (14)	Eq. (15)	IBSD	
	μ_1 (m)	σ_1^2 (m^2)	μ_2 (m)	σ_2^2 (m^2)	μ_3 (m)	σ_3^2 (m^2)	$E[V]$ (m^3)	Var[V] (m^6)	F(E[V]) (%)	$V_{99\%}$ (m^3)
Cube	1	0.25	1	0.25	1	0.25	1	0.95	79	4.54
	1	0.36	1	0.36	1	0.36	1	2.31	86	5.49
	1.71	0.25	1.71	0.25	1.71	0.25	5	6.98	71	12.86
Prism	1	0.25	2	0.25	2.5	0.25	5	9.53	72	16.06

tendency towards concentration on the right side. As expected, the special case representative of the convergence point of the shape domains in the classification diagram (B2) shows behavior in between the blade-like (B3) and the slab-like block (B4).

Regarding kinetic energy, the maximum value depicted in Fig. 18 for the 5 m^3 cube reference is 5000 kJ. The kinetic energies for the different blocks simulated in the second set of numerical simulations show that, in general, the reference value is one order of magnitude higher. In particular, block B2 has a reference maximum value twice the cubic block (1×10^4 kJ), while for both B5 and B3, it

is four times (2×10^4 kJ). Block B4 has a reference maximum value three times the cube (1.5×10^5 kJ). This shows that the shape also influences the kinetic energy of the block. In general, block shape influences significantly block motion, both in its geometric aspects, such as trajectories and runout, and in its energetic aspect.

4.4. Discussion on the effect of the uncertainties

Table 6 reports some practical examples quantifying the effect of uncertainty. The first example concerns a cubic block generated by three discontinuity sets with the same spacing PDF (seventh row in Table 1). $E[V]$ and Var$[V]$ are calculated with Eqs. (14) and (15) (seventh row in Table 2), and the volume CDF, namely IBSD, is calculated. Two descriptors of the IBSD are defined and used for comparing the cases: cumulative frequency corresponding to $E[V]$, called $F(E[V])$, and volume corresponding to 99% cumulative frequency, called $V_{99\%}$. They are both obtained directly from the IBSD. $F(E[V])$ represents the probability of not exceeding $E[V]$. $V_{99\%}$ is a parameter describing the amplitude of the IBSD, truncated at 99% of cumulative frequency.

The second case in Table 6 differs from the first one only in σ^2, which is larger. This causes an increase in Var$[V]$, $F(E[V])$, and $V_{99\%}$, which means that volume distribution is more dispersed, and the amplitude of the IBSD increases.

The third case is still a cube, with a bigger value of μ (1.71 times larger) and therefore of $E[V]$ (5 times larger) and Var$[V]$ (7.3 times larger), with respect to the first case. $F(E[V])$ is lower, meaning that the probability of not exceeding $E[V]$ is lower, and $V_{99\%}$ is 2.8 times larger.

The fourth case is a prismatic block, with the same $E[V]$ as the third case: $F(E[V])$ is similar, while $V_{99\%}$ is 1.2 times larger.

5. Conclusions

The assessment of the volumes of potentially detachable blocks from a rock slope is fundamental for a rigorous approach of rockfall phenomena, especially considering that most of the design methods available for countermeasures are based on energetic approaches.

(1) The evolution of non-contact measuring techniques allows the acquisition of increasingly large datasets of the rock discontinuity geometrical features. The use of statistical tests for the evaluation of the best-fitting distributions is strongly encouraged to reduce epistemic errors in surveyed data (i.e. orientation and spacing) and, therefore, the propagated errors on derived data (i.e. volume).

(2) The determination of the IBSD enables researchers to overcome the former concept of a so-called “characteristic block”, which is a deterministic value not able to consider the variability of the involved parameters. Specific equations have been developed in this study to compute the expected value and variance of the block volume for the case of a block generated by three discontinuity sets. The IBSD and the associated block shape distribution have been constructed through Monte Carlo simulations, considering different levels of uncertainty on spacing data. Moreover, the variability of block shape within the same IBSD was demonstrated. However, the equations proposed in this paper cannot be used directly in cases where the number of discontinuity sets is more than three. A reasonable solution would be to select combinations of three sets and evaluate their effects one at a time, assessing the global effect as a sort of sum of the contributions.

(3) The design of countermeasures for rockfall phenomena can be supported by the developed methods in evaluating the kinetic energy distribution (as a direct consequence of the IBSD knowledge) and optimizing their location, taking into account the estimation of block shape.

Declaration of competing interest

The authors declare that they have no known competing financial interests or personal relationships that could have appeared to influence the work reported in this paper.

List of symbols

S	Spacing, intended for both a deterministic value and a continuous random variable
μ	Expected value (mean) of spacing (coincident with E[S])
σ^2	Variance of spacing (coincident with Var[S])
N	Number of data in the spacing sample
V	Volume
$E[V]$	Expected value (mean) of volume
Var$[V]$	Variance of volume
$f(x)$	Probability density function (PDF) of a continuous random variable x
$F(x) = P(X \leq x)$	Cumulative distribution function (CDF) of a continuous random variable x
K	Fisher constant, the precision parameter of the Fisher distribution
θ	Angle from the true mean, in the Fisher distribution
K_i, K_j, K_k	Discontinuity sets
$\overrightarrow{\mu_i}, \overrightarrow{\mu_j}, \overrightarrow{\mu_k}$	Director vectors of the three discontinuity sets generating the block
S_i, S_j, S_k	Spacing of the three discontinuity sets generating the block
γ_{ij}, γ_{jk}, γ_{ki}	Angles between pairs of discontinuity sets generating the block
$\delta_{k\text{-}ij}$	Angle between $\overrightarrow{\mu_k}$ and $\overrightarrow{l_{ij}}$
$\overrightarrow{l_{ij}}$	Direction of the normal to $\overrightarrow{\mu_i}$ and $\overrightarrow{\mu_j}$
q	Dimensionless number that depends only on the shape of the block
Lo	Length of the longest edge of the block
In	Length of the intermediate edge of the block
Sh	Length of the shortest edge of the block
k	Shape factor
w	Width of the fallen compartments
α	First dimensional parameter describing shape
β	Second dimensional parameter describing shape
a	Shape parameter of the Gamma distribution
b	Scale parameter of the Gamma distribution
d	Fragment maximum dimension
R_n	Normal restitution coefficient
d_1, d_2, d_3	Main diameters of the simulated block
$F(E[V])$	Cumulative frequency corresponding to $E[V]$
$V_{99\%}$	Volume corresponding to 99% cumulative frequency in IBSD

References

Annavarapu, S., Kemeny, J., Dessureault, S., 2012. Joint spacing distributions from oriented core data. Int. J. Rock Mech. Min. Sci. 52, 40–45.
Baecher, G.B., Christian, J.T., 2003. Reliability and Statistics in Geotechnical Engineering, first ed. Wiley, Hoboken, New Jersey, USA.
Butler, R.F., 1992. Paleomagnetism: Magnetic Domains to Geologic Terranes. Blackwell Science, Boston, USA (Chapter 6)).
Carriero, M.T., Ferrero, A.M., Migliazza, M.R., Umili, G., 2021. Comparison between methods for calculating the volume of rock blocks. IOP Conf. Ser. Earth Environ. Sci. 833, 012049.

Carriero, M.T., Ferrero, A.M., Migliazza, M.R., Umili, G., 2023. Effect of uncertainties on block volume estimation. IOP Conf. Ser. Earth Environ. Sci. 1124, 012005.
Caviezel, A., Ringenbach, A., Demmel, S.E., et al., 2021. The relevance of rock shape over mass—implications for rockfall hazard assessments. Nat. Commun. 12, 5546.
DiFrancesco, P.M., Bonneau, D.A., Hutchinson, D.J., 2021. Computational geometry-based surface reconstruction for volume estimation: a case study on magnitude-frequency relations for a LiDAR-derived rockfall inventory. Int. J. Geo-Information 10 (3), 157.
Dorren, L.K.A., 2016. Rockyfor3D (v5.2) revealed – transparent description of the complete 3D rockfall model. ecorisQ paper. www.ecorisq.org.
Ferrero, A.M., Migliazza, M.R., Pirulli, M., Umili, G., 2016. Some open issues on rockfall hazard analysis in fractured rock mass: problems and prospects. Rock Mech. Rock Eng. 49, 3615–3629.
Ferrero, A.M., Umili, G., Migliazza, M.R., 2015. Some open issues on the design of protection barriers against rockfall. In: 49th US Rock Mechanics/Geomechanics Symposium 2015, pp. 3104–3109.
Fisher, R.A., 1953. Dispersion on a sphere. Proc. Roy. Soc. Lond. A 217, 295–305.
Hantz, D., 2011. Quantitative assessment of diffuse rock fall hazard along a cliff foot. Nat. Hazards Earth Syst. Sci. 11, 1303–1309.
ISRM, 1978. International society for rock mechanics commission on standardization of laboratory and field tests. Suggested methods for the quantitative description of discontinuities in rock masses. Int. J. Rock Mech. Min. Sci. 15 (6), 319–368.
Kalenchuk, K.S., Diederichs, M.S., McKinnon, S., 2006. Characterizing block geometry in jointed rockmasses. Int. J. Rock Mech. Min. Sci. 43 (8), 1212–1225.
Kalenchuk, K.S., McKinnon, S., Diederichs, M.S., 2008. Block geometry and rockmass characterization for prediction of dilution potential into sub-level cave mine voids. Int. J. Rock Mech. Min. Sci. 45 (6), 929–940.
Kemeny, J., Post, R., 2003. Estimating three-dimensional rock discontinuity orientation from digital images of fracture traces. Comput. Geosci. 29 (1), 65–77.
Kong, D.H., Wu, F.Q., Saroglou, C., 2020. Automatic identification and characterization of discontinuities in rock masses from 3D point clouds. Eng. Geol. 265, 105442.
Leine, R.I., Capobianco, G., Bartelt, P., Christen, M., Caviezel, A., 2021. Stability of rigid body motion through an extended intermediate axis theorem: application to rockfall simulation. Multibody Syst. Dyn. 52, 431–455.
Leine, R.I., Schweizer, A., Christen, M., Glover, J., Bartelt, P., Gerber, W., 2014. Simulation of rockfall trajectories with consideration of rock shape. Multibody Syst. Dyn. 32, 241–271.
Lu, P., Latham, J.P., 1999. Developments in the assessment of in-situ block size distributions of rock masses. Rock Mech. Rock Eng. 32, 29–49.
Macciotta, R., Gräpel, C., Skirrow, R., 2020. Fragmented rockfall volume distribution from photogrammetry-based structural mapping and discrete fracture networks. Appl. Sci. 10 (19), 6977.
Mavrouli, O., Corominas, J., 2017. Comparing rockfall scar volumes and kinematically detachable rock masses. Eng. Geol. 219, 64–73.
Mavrouli, O., Corominas, J., Jaboyedoff, M., 2015. Size distribution for potentially unstable rock masses and in situ rock blocks using LIDAR-generated digital elevation models. Rock Mech. Rock Eng. 48, 1589–1604.
Moos, C., Bontognali, Z., Dorren, L., Jaboyedoff, M., Hantz, D., 2022. Estimating rockfall and block volume scenarios based on a straightforward rockfall frequency model. Eng. Geol. 309, 106828.
Noël, F., Cloutier, C., Jaboyedoff, M., Locat, J., 2021. Impact-Detection Algorithm that uses point clouds as topographic inputs for 3D rockfall simulations. Geosciences 11 (5), 188.
Noël, F., Cloutier, C., Turmel, D., Locat, J., 2016. Using Point Clouds as Topography Input for 3D Rockfall Modeling. Landslides and Engineered Slopes. Experience, Theory and Practice. CRC Press, Napoli, Italy.
Odonne, F., Lézin, C., Massonnat, G., Escadeillas, G., 2007. The relationship between joint aperture, spacing distribution, vertical dimension and carbonate stratification: an example from the Kimmeridgian limestones of Pointe-du-Chay (France). J. Struct. Geol. 29 (5), 746–758.
Palmstrøm, A., 1995. RMI—a Rock Mass Characterization System for Rock Engineering Purposes. PhD Thesis. Oslo University, Norway.
Palmstrøm, A., 1996. Characterizing rock masses by the RMi for use in practical rock engineering. Tunn. Undergr. Space Technol. 11 (2), 175–188.
Palmstrøm, A., 2001. Measurement and characterization of rock mass jointing. In: Sharma, V.M., Saxena, K.R. (Eds.), In-situ Characterization of Rocks. Balkema, Rotterdam, pp. 49–97.
Priest, S.D., 1993. Discontinuity Analysis for Rock Engineering. Chapman & Hall, London.
Regione Piemonte, 2011. Digital Terrain Model. https://www.geoportale.piemonte.it/geonetwork/srv/ita/catalog.search#/metadata/r_piemon:224de2ac-023e-441c-9ae0-ea493b217a8e.
Riquelme, A., Cano, M., Tomás, R., Abellán, A., 2017. Identification of rock slope discontinuity sets from laser scanner and photogrammetric point clouds: a comparative analysis. Proc. Eng. 191, 838–845.
Ruiz-Carulla, R., Corominas, J., Mavrouli, O., 2017. A fractal fragmentation model for rockfalls. Landslides 14, 875–889.
Ruiz-Carulla, R., Corominas, J., Mavrouli, O., 2015. A methodology to obtain the block size distribution of fragmental rockfall deposits. Landslides 12, 815–825.
Santana, D., Corominas, J., Mavrouli, O., Garcia-Sellés, D., 2012. Magnitude-frequency relation for rockfall scars using a terrestrial laser scanner. Eng. Geol. 145, 50–64.
Stavropoulou, M., 2014. Discontinuity frequency and block volume distribution in rock masses. Int. J. Rock Mech. Min. Sci. 65, 62–74.
Umili, G., Bonetto, S.M.R., Mosca, P., Vagnon, F., Ferrero, A.M., 2020. In situ block size distribution aimed at the choice of the design block for rockfall barriers design: a case study along gardesana road. Geosciences 10 (6), 223.
van Veen, M., Hutchinson, D.J., Kromer, R., Lato, M., Edwards, T., 2017. Effects of sampling interval on the frequency - magnitude relationship of rockfalls detected from terrestrial laser scanning using semi-automated methods. Landslides 14, 1579–1592.
Wang, H., Latham, J.P., Poole, A.B., 1993. In-situ block size assessment from discontinuity spacing data. Int. J. Rock Mech. Min. Sci. Geomech. Abstr. 30 (2), A106.
Wang, H., Latham, J.P., Poole, A.B., 1991. Predictions of block size distribution for quarrying. Q. J. Eng. Geol. Hydrogeol. 24 (1), 91–99.
Wang, X.L., Frattini, P., Crosta, G.B., et al., 2014. Uncertainty assessment in quantitative rockfall risk assessment. Landslides 11, 711–722.

Gessica Umili is currently an Associate Professor at the University of Turin, Italy. She received a Ph.D. degree from the University of Parma, Italy. Her research focuses on rock mechanics and slope stability supported by remotely sensed data. Gessica Umili has extensive experience in non-contact survey methods for geomechanical purposes. She has developed a method for automatic discontinuity traces mapping and sampling on rock mass 3D models, aiming to calculate the degree of fracturing and the intensity of rock discontinuities. At present, she is investigating the rockfall phenomenon, with a particular focus on block volume distributions and the identification of source areas. She is also involved in developing design strategies for rockfall barriers. She has published more than 10 high-impact Q1 journal articles. In 2021 she was invited to give a lecture within the ISRM Course on Rock Mass Characterization and Monitoring based on Advanced Remote Sensing Techniques coordinated by Prof. Leandro Alejano.